

Original Article

Biodistribution of intravenous [^{99m}Tc]Tc-phytate in mouse models of chemically and foreign-body induced sterile inflammation

Maria Papachristou^{1*}, Dimitrios Priftakis², Stavros Xanthopoulos^{3*}, Ioannis Datselis^{1*}, Penelope Bouziotis^{3*}

¹Nuclear Medicine and PET/CT Department, General Hospital of Athens "Evangelismos", Athens, Greece; ²Institute of Nuclear Medicine, University College London Hospital, London, United Kingdom; ³Radiochemical Studies Laboratory, Institute of Nuclear & Radiological Sciences & Technology, Energy & Safety, National Center for Scientific Research "Demokritos", Athens, Greece. *Equal contributors.

Received August 22, 2021, Accepted June 5, 2022; Epub June 15, 2022; Published June 30, 2022

Abstract: When injected intravenously, [^{99m}Tc]Tc-phytate forms particles in the nanometer range. This size can favor its extravasation into tumor and inflammation through pores of the vasculature. The aim of this work is the evaluation of the use of [^{99m}Tc]Tc-phytate to assess sterile inflammation in mouse models. Biodistribution studies of [^{99m}Tc]Tc-phytate were performed in two groups of male Swiss Albino mice. Sterile inflammation was induced after intramuscular injection of turpentine in the first group (chemically induced sterile inflammation model) and after implantation of sterile metal bolts in the second group (foreign-body induced sterile inflammation model). [^{99m}Tc]Tc-phytate was intravenously injected after the development of inflammation in both groups and *ex vivo* biodistribution of the radiolabelled complex followed at different time-points. Biodistribution was expressed as percent injected dose per gram (%ID/g). Target-to-background ratios were also recorded. For the chemically induced sterile inflammation model, *ex vivo* biodistribution evaluation measurements revealed a pronounced uptake in the inflamed muscle when compared to uptake in the control/non-inflamed muscle. Moreover, as expected, there is a high uptake in the liver and spleen. For the foreign-body induced sterile inflammation model, a significantly higher uptake was observed in the inflamed muscle post [^{99m}Tc]Tc-phytate injection, both for the 24 hours post-bolt implantation and for the 7 days post-bolt implantation groups. The nanoparticle properties of [^{99m}Tc]Tc-phytate are potentially useful in the imaging of different types of sterile inflammation with translational potential clinical SPECT (single photon emission computed tomography) imaging applications in humans.

Keywords: Technetium Tc 99m, phytate, inflammation, foreign-body reaction, radionuclide imaging, nanoparticles, preclinical

Introduction

[^{99m}Tc]Tc-phytate was first introduced by Subramanian et al. in 1973 as a non-colloidal agent which, when injected intravenously, forms small particles *in vivo* by interaction with calcium and other cationic metals [1]. These particles have demonstrated extraction from the circulation via phagocytosis by the cells of the reticuloendothelial system (RES), mainly in the liver, spleen and bone marrow [2]. Based on this mechanism, [^{99m}Tc]Tc-phytate may be used as an alternative to [^{99m}Tc]Tc-sulfur colloid or radiolabeled nanocolloids in liver imaging, mainly for suspected focal nodular hyperplasia [3], bone marrow imaging (e.g. in conjunction with

radiolabeled leukocytes for prosthetic joint infections [4]) and lymphoscintigraphy/sentinel lymph node identification [5].

However, new information has emerged over the decades which has led to the consideration of [^{99m}Tc]Tc-phytate as a radiolabeled nanoparticle tracer with potential new applications [6, 7]. First, the size of the particles has been found to fall within the nanoparticle range [8, 9]. Second, the RES has evolved to the mononuclear phagocyte system (MPS), a newly described organic entity which is comprised of all categories of phagocytic cells in the body, both stationary in various organs (e.g. liver, spleen, bone marrow etc.) or circulating in the

bloodstream. Examples of cell types participating in the MPS are the monocytes, the macrophages, and the dendritic cells, which play an important role in the immune response [9]. Third, the recent quest for nanoparticle-based drugs or drug delivery systems has brought forth the concept of the Enhanced Permeation and Retention (EPR) effect, which is the hypothesized mechanism by which nanoparticles are delivered in inflammatory, infectious and tumor lesions through appropriately-sized leaks in the vasculature that allow the passage of the nanoparticles and their subsequent phagocytosis by cells present in these types of lesions [10, 11].

Based on the information provided by recent literature, the experiments presented in this article were designed with the aim to evaluate the ability of [^{99m}Tc]Tc-phytate to assess different types of sterile inflammation induced either by a chemical or a foreign body in preclinical animal models through the nanoparticle properties of the radiolabeled tracer.

Materials and methods

All chemicals employed for this research were analytical grade. MeOH was purchased from Aldrich, USA. The ^{99m}Tc generator was purchased from GE Healthcare. Saline was purchased from Demo (Athens, Greece).

Biodistribution studies were performed using normal Swiss mice (20±2 g) of the same colony and age, purchased from the Breeding Facilities of the Institute of Biosciences and Applications NCSR “Demokritos”.

Ethics approval

Animal experiments were carried out according to European and national regulations. These studies have been further approved by the Ethics Committee of the NCSR “Demokritos”. Animal care and procedures followed are in accordance with institutional guidelines and licenses issued by the Department of Agriculture and Veterinary Policies of the Prefecture of Attiki (Registration Numbers: EL 25 BIO 022 and EL 25 BIO 021).

Radiolabelling of phytate and radiochemical purity

[^{99m}Tc]Tc-phytate was prepared by reconstitution of a commercial cold kit (Phytacis, IBA

Molecular). An aliquot of 370 MBq of sodium [^{99m}Tc]pertechnetate (VII) was added to the vial and the solution was kept at room temperature (RT) for 15 min.

For quality control, the radiochemical yield was assessed by Thin-Layer Chromatography (TLC), as described in the Summary of Product Characteristics (SPC), using Whatman 1 mm strips with a two-solvent system: methanol and 0.9% NaCl (80/20 v/v) as the solvent system. The radiolabelled product was kept at RT before use.

Ex vivo biodistribution studies

All applicable institutional and/or national guidelines for care and use of animals were followed. Mice were housed under constant environmental conditions with 12 h light-dark cycles and had free access to food and water.

Chemical-induced sterile inflammation animal model

For the induction of inflammation, Swiss Albino mice were inoculated with 50 µL of pure turpentine oil in the left thigh muscle under slight ether anaesthesia [12, 13]. All animals developed an oedema 18 to 24 h after turpentine inoculation, which was visible to the naked eye.

Ex vivo animal experiments were performed in the animals with chemical-induced inflammation (20±2 g, n=9 animals). First, the animals were injected with 100 µL (3.7 MBq/0.1 mCi) of ^{99m}Tc-Phytate via the tail vein. Animals were sacrificed by cardiectomy under slight isoflurane anaesthesia at 1, 2, and 4 h post injection (n=3 animals per time-point). The different time points were selected in order to look for potential significant redistribution of the tracer, which would favour a specific time-point over the others for the identification of sterile inflammation. The main tissues and organs (blood, heart, liver, stomach, intestines, spleen, lungs, pancreas, and bones) were excised, blotted dry and weighed. The inflamed thigh was excised and trimmed of the neighbouring subcutaneous tissue. The muscle of the non-inflamed right thigh was also excised, for reasons of comparison. A standard was prepared from the injected radiotracer and was counted each time simultaneously with the tissues excised, allowing for measurements to be corrected for physical decay of the radioisotope. [^{99m}Tc]

Tc-phytate in inflammation

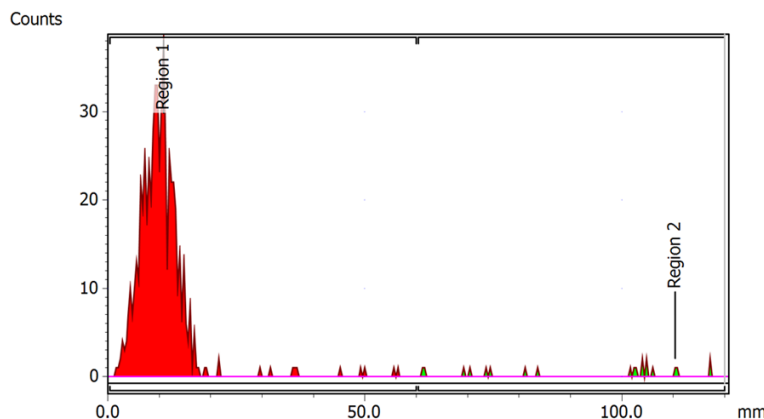


Figure 1. TLC chromatogram of ^{99m}Tc labeling of Phytate - Solvent system: MeOH:H₂O 80:20. In this system, the Rf of [^{99m}Tc]Tc-phytate is 0, while the Rf of uncomplexed ^{99m}Tc is 1.

Tc-phytate distribution over time was expressed as injected dose per gram (%ID/g).

Sterile biomaterial inflammation animal model

For the second experiment, sterile inflammation was induced with implantation of dry-sterilized stainless-steel bolts (180°C, 3 h). Before implantation, the mice were anaesthetized with a mixture of ketamine/xylazine. An incision was carefully made in the left hind leg of each mouse, and one bolt was implanted.

Foreign-body-induced inflammation by biomaterials was assessed at 24 and 168 h post-implantation (n=6, i.e. 3 mice per time-point), by injection of [^{99m}Tc]Tc-phytate (100 μL , 3.7 MBq/0.1 mCi) via the tail vein. The time points were selected according to the pathophysiology of foreign body reaction where the persistence of the stimulus leads to prolonged inflammatory response, in order to detect any differences in the early and late presence of radiolabelled particles at the site of inflammation. Animals were sacrificed by cardiectomy under slight isoflurane anaesthesia at 2 h post-injection, and the main tissues and organs (blood, heart, liver, stomach, intestines, spleen, lungs, pancreas and bones) were excised, blotted dry and weighed. The inflamed thigh was excised and trimmed of the neighbouring subcutaneous tissue. The muscle of the non-inflamed right thigh was also excised, for reasons of comparison. A standard was prepared and measured along with the tissue/organ samples, for reasons mentioned above. [^{99m}Tc]Tc-phytate distri-

bution over time was expressed as injected dose per gram (%ID/g).

Results

Results of the TLC and Quality Control of the radiolabelling:

1. PH=6. 2. Radiochemical purity = $98 \pm 0.5\%$, Rf of [^{99m}Tc]Tc-Phytate is 0, while the Rf of uncomplexed ^{99m}Tc is 1 (**Figure 1**). 3. Stability of the complex up to 6 h (as recommended in its SPC).

Chemical-induced sterile inflammation animal model

Ex vivo biodistribution evaluation revealed higher mean [^{99m}Tc]phytate uptake in the inflamed thigh compared to mean uptake in the control tissue/non-inflamed thigh at all time points as follows:

1 hour post injection: $0.44 \pm 0.07\%$ ID/g versus $0.14 \pm 0.08\%$ ID/g, ratio: 3.1:1; 2 hours post injection: $0.48 \pm 0.12\%$ ID/g versus $0.20 \pm 0.14\%$ ID/g, ratio 2.4:1; 4 hours post injection: $0.25 \pm 0.06\%$ ID/g versus $0.16 \pm 0.06\%$ ID/g, ratio 1.5:1.

It is evident from the above values that the inflamed thigh: non-inflamed thigh (control thigh) ratio was higher at 1 hour post-injection. Moreover, there is a high uptake in the liver and spleen, as expected from the known biodistribution of [^{99m}Tc]Tc-phytate. The results are presented in **Figures 2 and 3**.

Sterile biomaterial inflammation animal model

After injection of [^{99m}Tc]Tc-phytate and euthanization at 2 h post-injection, mean uptake values at the site of implantation versus the mean uptake at the non-inflamed muscle were:

At 1 day post-bolt implantation: $1.13 \pm 0.20\%$ ID/g versus $0.34 \pm 0.06\%$ ID/g, ratio 3.3:1. At 7 days post-implantation, $1.33 \pm 0.09\%$ ID/g versus $0.29 \pm 0.08\%$ ID/g, ratio 4.6:1. (**Figures 4 and 5**).

It is evident from the above values that there is a higher inflamed/non-inflamed thigh ratio for the mice bearing bolts, at 1 day and 7 days post-bolt implantation (3.28 ± 0.10 and

Tc-phytate in inflammation

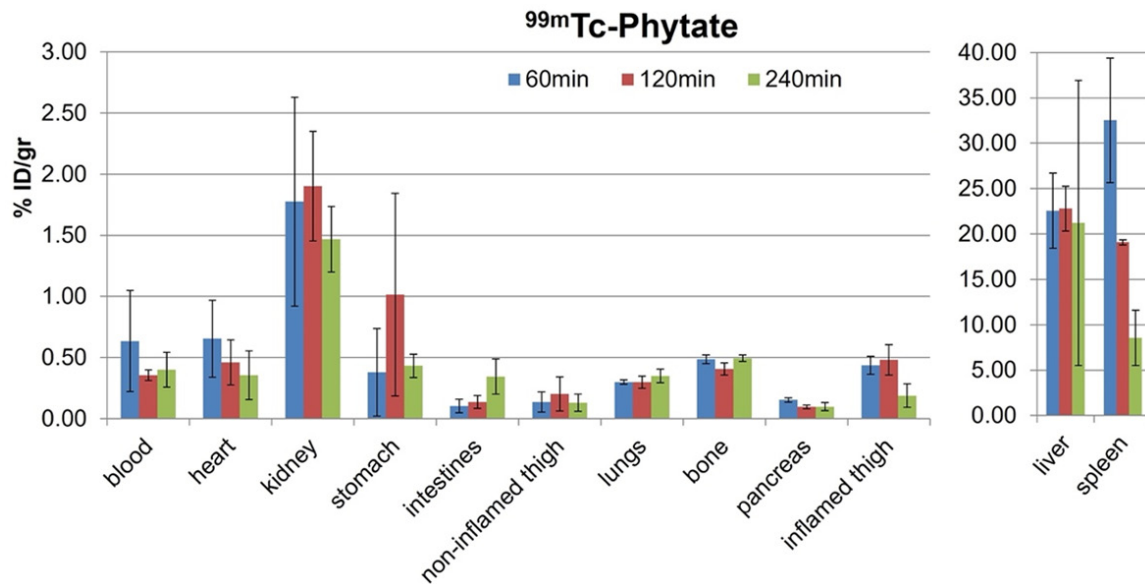


Figure 2. Results of ^{99m}Tc -phytate biodistribution in the chemical-induced sterile inflammation animal model. High activity is observed in the liver, spleen and kidney, representing the physiological distribution of ^{99m}Tc -phytate. Activity in the inflamed thigh is significantly higher than in the non-inflamed counterpart at all time points.

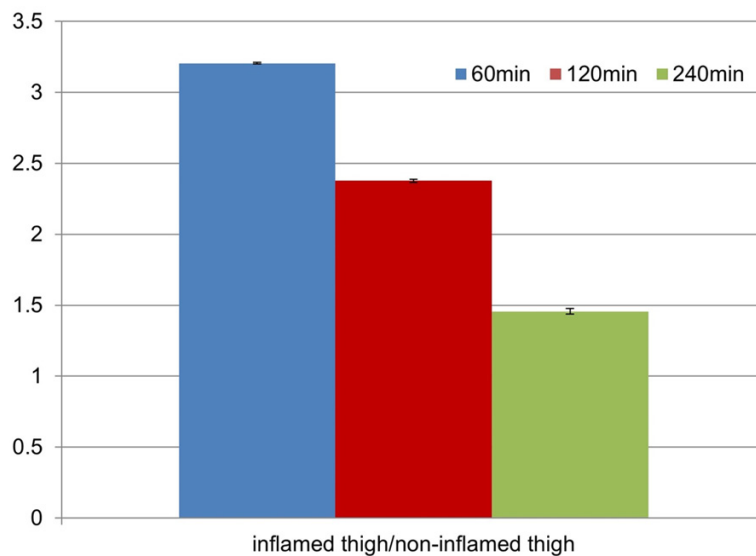


Figure 3. Chemical-induced sterile inflammation animal model. Inflamed thigh to non-inflamed thigh ^{99m}Tc -phytate uptake ratios at 1, 2 and 4 hours post-injection. The ratio is higher at 1 hour post-injection.

4.66±0.005, respectively), in comparison to the chemical-induced model (2.38±0.01). We also observed an increase in radiotracer uptake in the inflamed/non-inflamed thigh ratio for the bolt model, from 1 day to 7 days, which may be attributed to ongoing inflammation, compatible with typical foreign-body reaction to biomaterial implantation, as previously described in lit-

erature [14, 15]. Finally, the absolute mean values of ^{99m}Tc -phytate uptake were higher in the foreign-body inflammation model in comparison to the chemical-induced inflammation model.

Discussion

In this study, we present the biodistribution of intravenously injected ^{99m}Tc -phytate in mice, and demonstrate that there is increased ^{99m}Tc -phytate uptake in sites of experimentally-induced sterile inflammation mice with a satisfactory target-to-nontarget ratio. Sterile inflammation is defined as the activation of the innate immune response by cellular damage in the absence of an infectious agent.

The causes of cellular damage that trigger sterile inflammation can be exogenous, such as trauma, chemical injury, foreign bodies or endogenous such as aberrant metabolic products, ischemia, and necrosis [16]. Our results are in agreement and expand on previously published results by Mota et al. [7], who reported increased ^{99m}Tc

Tc-phytate in inflammation

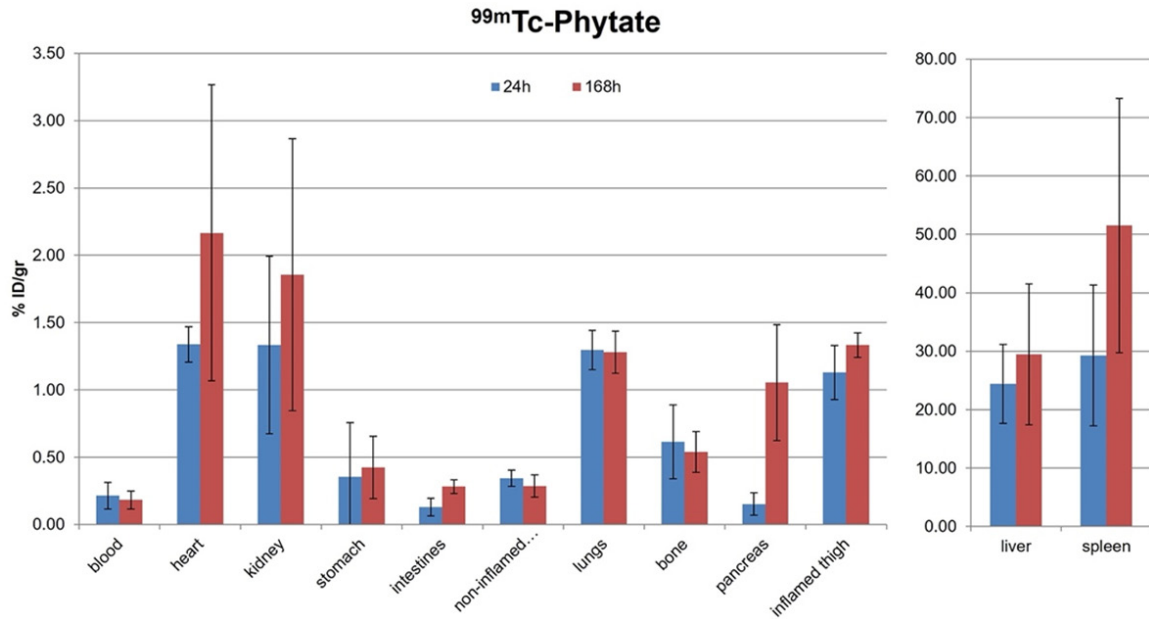


Figure 4. Results of ^{99m}Tc -phytate biodistribution in the biomaterial sterile inflammation animal model. High activity is observed in the liver, spleen and kidney representing the physiological distribution of ^{99m}Tc -phytate. Activity in the inflamed thigh is significantly higher than in the non-inflamed counterpart in both groups of mice.

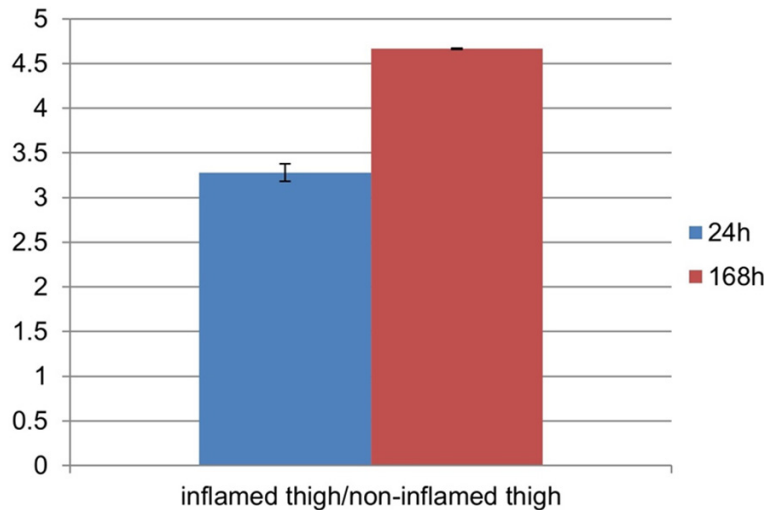


Figure 5. Biomaterial sterile inflammation animal model. Inflamed thigh to non-inflamed thigh ^{99m}Tc -phytate uptake ratio at 1 day and 7 days post-implantation. The ratio is higher at 7 days after biomaterial implantation.

Tc-phytate uptake in images acquired from a zymosan-induced sterile inflammation rat model. In our experiments, instead of zymosan which is a large biomolecule consisting of protein-carbohydrate complexes, intramuscular turpentine injection was used as an agent of chemical injury as well as intramuscular implantation of a metallic bolt, in order to elicit a for-

eign body reaction. Therefore, our study does not only prove the reproducibility of the results provided by the study of Mota et al., but it provides further evidence that ^{99m}Tc Tc-phytate may be a useful imaging agent for any type of sterile inflammation, independently of the cause.

The mean target-to-nontarget uptake ratio of ^{99m}Tc -phytate reached 3.1:1 for the chemical-induced sterile inflammation model, and 4.6:1 for the foreign-body-induced sterile inflammation model. These ratios are thought to represent high enough contrast for lesion detectability in

imaging, although this is also influenced by a multitude of factors, such as the size of the lesion and the resolution of the imaging instrumentation. Therefore, direct comparison between the mean uptake ratios in our models and the values reported by Mota et al. (up to 10.24:1 [7]) is not reliable. However, based on our results, it is reasonable to speculate that

Tc-phytate in inflammation

[^{99m}Tc]Tc-phytate uptake varies between different types of sterile inflammation and may be more suitable for imaging certain aetiologies.

Moreover, comparison between timepoints of imaging show that early imaging (1-2 hours post-injection) is optimal and results in higher target-to-nontarget uptake ratio for all models. On the other hand, the optimal time for imaging after the stimulus that causes inflammation depends on the stimulus itself and the natural history of the reaction elicited. This is better highlighted in the foreign-body-induced sterile inflammation model, where the persistence of the stimulus, which is the foreign body, leads to a long-lasting response with accumulation of inflammatory cells and formation of giant cell tissue around the foreign body which may last for more than 2 weeks [14, 15]. Indeed, our measurements show that delayed assessment with [^{99m}Tc]Tc-phytate at 7 days after implantation results in a higher uptake ratio than assessment 1 day post-implantation.

The biodistribution of [^{99m}Tc]Tc-phytate is characterized by the high uptake in the liver and the spleen in keeping with the known mechanism of phagocytosis of the particles that phytate forms with calcium and other cations when injected intravenously by MPS cells [1]. Nanoparticles have been shown to be taken up and cleared by a variety of liver cells, mainly Kupffer cells, but also hepatic B cells and sinusoidal endothelial cells, while attenuation of nanoparticles in the spleen is mainly due to macrophage populations [17, 18]. It seems reasonable to speculate that the [^{99m}Tc]Tc-phytate particles are distributed to the same cell populations in these organs, although no histopathologic confirmation for [^{99m}Tc]phytate has been reported to our knowledge. The particle nature of [^{99m}Tc]Tc-phytate, which falls within the nanoparticle range [8, 9] is most likely responsible for the demonstrated accumulation of this tracer at sites of sterile inflammation. Specifically, during the inflammatory response vasodilation occurs and irregular openings appear in the vascular endothelium, which are wide enough to allow the passage of intravenously-injected nanoparticles. This creates an enhanced permeation effect that contributes to the increased concentration of nanoparticles in inflammatory lesions [19-21].

The increased vascular leakage results in the rapid delivery of the body's innate defences to

the offended site, such as antibodies, complement, granulocytes and monocytes. The latter cellular components are phagocytic cells of the mononuclear phagocyte system (MPS), which also can internalize the nanoparticles that have already leaked through the endothelial openings. This is described as enhanced retention effect and combined with the enhanced permeation, gives rise to the concept of the enhanced permeation and retention (EPR) effect which is believed to be the main mechanism that drives the delivery of nanoparticles in inflammatory lesions. Similarly, the EPR effect is thought to be also manifested in cancer [19-21]. The EPR effect can therefore explain the increased lesion distribution of [^{99m}Tc]Tc-phytate, which having the size of a nanoparticle accumulates in the sites of sterile inflammation.

Despite the undeniable success of the EPR effect concept in explaining and predicting the distribution of a plethora of nanoparticle-based anti-tumour drugs [22], there have been publications that challenge some aspects of this phenomenon [23, 24]. It has been proposed that the description of the EPR effect encompasses a multitude of mechanisms, particularly in tumours with complex biology [25].

Another discussed limitation is the low specificity of the phenomenon, as nanoparticles are not preferentially taken up by the target only, but there is high physiological uptake in large organs such as the liver, spleen and bone marrow [23]. Indeed, our results demonstrate that despite the significantly higher [^{99m}Tc]Tc-phytate uptake at the inflammatory site, it is only a small proportion of the injected tracer that reaches the target lesion. According to the biodistribution, the largest ratio of the radio-tracer is retained by the liver and the spleen. A possible way to bypass this issue may be the injection of cold nanoparticles before the radio-labelled tracer injection, which might reduce the ability of the liver and the spleen to take up [^{99m}Tc]Tc-phytate resulting in higher relative distribution to the target [26]. Further experiments need to be performed to prove the feasibility and efficiency of this approach.

The results of our study indicate that [^{99m}Tc]Tc-phytate, having properties such as particle formation in the circulation after injection with the appropriate size, satisfactory uniformity, neutral charge and circulation time of approxi-

mately 3 minutes that allows for early imaging, may be a suitable radiotracer for nanoparticle-based SPECT imaging of inflammation. Clinically relevant examples of human diseases where sterile inflammation plays a significant role, apart from the demonstrated foreign-body reaction, are type 2 diabetes, endometriosis and fungal infections, among others [16].

The most extensively studied nanoparticle-based imaging agents are superparamagnetic iron oxide nanoparticles (SPIONs) which are used as contrast agents for MRI [27]. In the field of radiopharmaceuticals, experimental PET-based radiopharmaceuticals are being developed labelled with isotopes such as ^{18}F , ^{64}Cu and ^{89}Zr [28]. It is unknown if [$^{99\text{m}}\text{Tc}$]Tc-phytate has comparable imaging results to the above-mentioned imaging agents. However, [$^{99\text{m}}\text{Tc}$]Tc-phytate has significant advantages such as low toxicity and proven safety for human use, commercial availability, and low cost.

Our study presents a number of limitations, the main one being the lack of *in vivo* imaging. The reason is that our group does not have access to small animal SPECT imaging, therefore we opted for the *ex vivo* biodistribution design. In this design, the measurement of the activity in the tissue requires the sacrifice of the animal, thus the sample size per time point was limited to 3 animals according to the “3Rs” principle (Replacement, Reduction and Refinement) for the humane use of animals in experiments [29]. This may indeed limit the statistical power of our quantitative analysis. However, the qualitative demonstration of significant [$^{99\text{m}}\text{Tc}$]phytate uptake at the sterile inflammation site in a total of 15 animals, including a variety of sterile inflammation models and time points, not only strongly corroborates and expands on the results of the only previous experiment in this setting [7], but is also predictive of increased likelihood of successful translation in future preclinical and clinical imaging studies.

A further limitation of the study is the lack of particle size measurement and particularly of the size range of particles preferentially trapped at the inflammation sites. According to previous studies on [$^{99\text{m}}\text{Tc}$]Tc-phytate, the particle size ranges from 5-1000 nm. Particles in the range of 300-1000 nm are preferentially withheld in the liver and spleen [30], therefore the majority of the remaining particles are likely to be up to

300 nm. Although the prevalent definition of nanoparticles sets a size threshold at 100 nm, in the case of pharmaceuticals, larger particles which have similar functional characteristics to nanoparticles may be considered as nanotechnological products according to the FDA [31]. Further studies with selected homogeneous radiolabelled nanoparticles could confirm the size of particles preferentially trapped at the inflammation site. Such a tracer will likely have better target-to-background ratio with less non-target uptake in the liver and spleen.

Conclusion

This study has succeeded to demonstrate that the nanoparticle properties of [$^{99\text{m}}\text{Tc}$]Tc-phytate are potentially useful in the imaging of different types of sterile inflammation, such as chemical-induced and foreign-body-induced sterile inflammation. The results of the preclinical animal experiments presented in this article, confirm and expand on previously published studies, which demonstrate that [$^{99\text{m}}\text{Tc}$]Tc-phytate has the right properties for safe and low-cost nanoparticle-based SPECT imaging of inflammation with various potential clinical translation applications in humans.

Disclosure of conflict of interest

None.

Address correspondence to: Dimitrios Priftakis, Institute of Nuclear Medicine, University College London Hospital, 235 Euston Road, London NW1 2BU, United Kingdom. Tel: +44 020 344 70560, +44 (0)7877035210; E-mail: dimitris.priftakis@nhs.net

References

- [1] Subramanian G, McAfee JG, Mehter A, Blair RJ and Thomas FD. $^{99\text{m}}\text{Tc}$ -stannous phytate: a new *in vivo* colloid for imaging the reticuloendothelial system. *J Nucl Med* 1973; 14: 459.
- [2] Alavi A, Staum MM, Shesol BF and Bloch PH. Technetium- $^{99\text{m}}$ stannous phytate as an imaging agent for lymph nodes. *J Nucl Med* 1978; 19: 422-426.
- [3] Hsu YL, Chen YW, Lin CY, Lai YC, Chen SC and Lin ZY. Variable uptake feature of focal nodular hyperplasia in Tc- $^{99\text{m}}$ phytate hepatic scintigraphy/single-photon emission computed tomography—a parametric analysis. *Kaohsiung J Med Sci* 2015; 31: 621-625.
- [4] Jung KP, Park JS, Lee AY, Choi SJ, Lee SM and Bae SK. The clinical usefulness of $^{99\text{m}}\text{Tc}$

Tc-phytate in inflammation

- HMPAO leukocyte/^{99m}Tc phytate bone marrow scintigraphy for diagnosis of prosthetic knee infection: a preliminary study. *Nucl Med Mol Imaging* 2012; 46: 247-253.
- [5] Yang SS, Bao WY, Bai XR, Gao C, Zhang BM and Jiang ZJ. ^{99m}Tc-labeled sodium phytate and stannous chloride injection accurately detects sentinel lymph node in axillary of early stage breast cancer: a randomized, controlled study. *Onco Targets Ther* 2018; 11: 1891-1898.
- [6] Fernandes RS, Mota LG, Kalbasi A, Moghbel M, Werner TJ, Alavi A, Rubello D, Cardoso VN and de Barros AL. ^{99m}Tc-phytate as a diagnostic probe for assessing inflammatory reaction in malignant tumors. *Nucl Med Commun* 2015; 36: 1042-1048.
- [7] Mota LG, de Barros AL, Fuscaldi LL, de Souza CM, Cassali GD, Moghbel M, Alavi A, Rubello D, Fernandes SO, Oliveira MC and Cardoso VN. Evolving role of radiolabeled particles in detecting infection and inflammation, preliminary data with ^{99m}Tc-phytate in rats. *Nucl Med Commun* 2015; 36: 1113-1119.
- [8] Paiva GR, Filho RS, Ferreira LM, Wagner J, Nogueira SA, Novo NF, Juliano Y and Rocha JL. Phytate technetium-^{99m} versus dextran 500 technetium-^{99m} in the sentinel lymph node biopsy. *Acta Radiol* 2006; 47: 65-70.
- [9] Yona S and Gordon S. From the reticuloendothelial to mononuclear phagocyte system - The unaccounted years. *Front Immunol* 2015; 6: 328.
- [10] Peer D, Karp JM, Hong S, Farokhzad OC, Margalit R and Langer R. Nanocarriers as an emerging platform for cancer therapy. *Nat Nanotechnol* 2007; 2: 751-760.
- [11] Maeda H. Macromolecular therapeutics in cancer treatment: the EPR effect and beyond. *J Control Release* 2012; 164: 138-144.
- [12] Mirzaei A, Jalilian AR, Akhlaghi M and Beiki D. Production of Ga⁶⁸-citrate based on SnO₂ generator for short-term turpentine oil-induced inflammation imaging in rats. *Curr Radiopharm* 2016; 9: 208-214.
- [13] Rivera S and Ganz T. Animal models of anemia of inflammation. *Semin Hematol* 2009; 46: 351-357.
- [14] Selvam S, Kundu K, Templeman KL, Murthy N and García AJ. Minimally invasive, longitudinal monitoring of biomaterial-associated inflammation by fluorescence imaging. *Biomaterials* 2011; 32: 7785-7792.
- [15] Anderson JM, Rodriguez A and Chang DT. Foreign body reaction to biomaterials. *Semin Immunol* 2008; 20: 86-100.
- [16] Rubartelli A, Lotze MT, Latz E and Manfredi A. Mechanisms of sterile inflammation. *Front Immunol* 2013; 4: 398.
- [17] Ray K. Clearance of nanomaterials in the liver. *Nat Rev Gastroenterol Hepatol* 2016; 13: 560.
- [18] Cataldi M, Vigliotti C, Mosca T, Cammarota MR and Capone D. Emerging role of the spleen in the pharmacokinetics of monoclonal antibodies, nanoparticles and exosomes. *Int J Mol Sci* 2017; 18: 1249.
- [19] Hashizume H, Baluk P, Morikawa S, McLean JW, Thurston G, Roberge S, Jain RK and McDonald DM. Openings between defective endothelial cells explain tumor vessel leakiness. *Am J Pathol* 2000; 156: 1363-1380.
- [20] Maeda H, Wu J, Sawa T, Matsumura Y and Hori K. Tumor vascular permeability and the EPR effect in macromolecular therapeutics: a review. *J Control Release* 2000; 65: 271-284.
- [21] Maeda H, Nakamura H and Fang J. The EPR effect for macromolecular drug delivery to solid tumors: improvement of tumor uptake, lowering of systemic toxicity, and distinct tumor imaging in vivo. *Adv Drug Deliv Rev* 2013; 65: 71-79.
- [22] Rosenblum D, Joshi N, Tao W, Karp JM and Peer D. Progress and challenges towards targeted delivery of cancer therapeutics. *Nat Commun* 2018; 9: 1410.
- [23] Nichols JW and Bae YH. EPR: evidence and fallacy. *J Control Release* 2014; 190: 451-464.
- [24] Nehoff H, Parayath NN, Domanovitch L, Taurin S and Greish K. Nanomedicine for drug targeting: Strategies beyond the enhanced permeability and retention effect. *Int J Nanomedicine* 2014; 9: 2539-2555.
- [25] Bolkestein M, de Blois E, Koelewijn SJ, Eggermont AM, Grosveld F, de Jong M and Koning GA. Investigation of factors determining the enhanced permeability and retention effect in subcutaneous xenografts. *J Nucl Med* 2016; 57: 601-607.
- [26] Liu T, Choi H, Zhou R and Chen IW. RES blockade: a strategy for boosting efficiency of nanoparticle drug. *Nano Today* 2015; 10: 11-21.
- [27] Neuwelt A, Sidhu N, Hu CA, Mlady G, Eberhardt SC and Sillerud LO. Iron-based superparamagnetic nanoparticle contrast agents for MRI of infection and inflammation. *AJR Am J Roentgenol* 2015; 204: W302-13.
- [28] Kamkaew A, Ehlerding EB and Cai W. Nanoparticles as radiopharmaceutical vectors. In: *Radiopharmaceutical Chemistry*. Lewis JS, Windhorst AD and Zeglis BM, editions. Springer International Publishing, Cham 2019. pp. 181-203.
- [29] Flecknell P. Replacement, reduction and refinement. *ALTEX* 2002; 19: 73-78.
- [30] Phytacis® Kit for the preparation of technetium [^{99m}Tc]phytate injection User Package Leaflet, 2017. <https://www.curiumpharma.com/wp-content/uploads/2018/05/T1800nH.pdf>.
- [31] Guidance for industry considering whether an FDA-regulated product involves the application of nanotechnology, U.S. Department of Health and Human Services, Food and Drug Administration, 2014.